Elastic Material Model Mismatch Effects in Deformable Motion Estimation

GJ Klein and RH Huesman

Center for Functional Imaging, Lawrence Berkeley National Laboratory
University of California, 1 Cyclotron Road, Berkeley, CA 94720

Abstract

Deformable motion models are useful for analysis of dynamic datasets exhibiting non-rigid motion, as in gated cardiac PET. We employ an algorithm that obtains a vector field to describe the relative motion of each voxel between two data sets. The estimation is based on a two-component cost function: an image matching component, and a motion field smoothness component. An important aspect of obtaining an accurate motion field estimate is properly balancing the weight between the two cost components. We show that by using a material elastic model inspired by continuum mechanics, an intuitive interpretation of the weighting factors for the smoothness constraint may be obtained. Further, we show that mismatches between actual material elastic parameters and those used by the estimation algorithm can lead to greater estimation error. Results are validated using an ellipsoidal phantom simulating compressible and incompressible deformations.

I. Introduction

Establishing a correspondence between voxels in two image volumes from a gated cardiac data acquisition is necessary to make wall motion estimates or calculations on matching tissue regions. Because the myocardium is a non-rigid structure that bends and stretches during the cardiac cycle, simple motion models such as a six parameter rigid-body description are inadequate to describe the motion, and a more complex deformable motion model must be used.

One technique to describe the motion is to use a dense vector field, called a motion field, which describes the relative displacement of each voxel, and thus establishes a voxel-by-voxel correspondence for every point in two image volumes. Algorithms to estimate this motion field find their roots in the two-dimensional optical flow literature. In simple terms, these algorithms are all based on two general constraints. First is an image matching constraint that serves as a driving force trying to pull voxels in a source volume so that they deform to match the image in a reference volume. The second constraint imposes a regularization on the motion field, and tries to restrict the large domain of possible deformations to those which are more smooth and more physically likely. For example, Song and Leahy [1] use a 3D generalization of an optical flow algorithm that expresses the regularization constraint in terms of two penalties. A general smoothness constraint penalizes large values in the gradient of the motion field, and the other constraint penalizes motion fields with non-zero divergence. A problem with this approach is that it is difficult *a priori* to choose factors which appropriately weight the two regularization components against each other. We address this problem by using a regularization function inspired by continuum mechanics. As the motion field deforms the source volume, it is penalized by the strain energy of a similarly deformed uniform elastic object. By choosing elastic parameters which are appropriate for the physical object being deformed, we can thus have better intuition regarding the appropriate weight of regularization components.

II. Method

The motion estimation framework is described as follows. Define two 3D density fields, a source volume, $f_1(\boldsymbol{r})$, and a reference volume, $f_2(\boldsymbol{r})$, where $\boldsymbol{r} = (x, y, z)$ represents the voxel index. A dense Lagrangian motion field is defined as $\boldsymbol{m}(\boldsymbol{r}) = (u(\boldsymbol{r}), v(\boldsymbol{r}), w(\boldsymbol{r}))$, and the deformed volume of f_1 is defined as $\hat{f}(\boldsymbol{r}) = f_1(\boldsymbol{r} + \boldsymbol{m})$. With these definitions, we can express an image matching error term, $e_I(\boldsymbol{r})$, given by

$$e_I(\boldsymbol{r}) = \gamma_I [f_2(\boldsymbol{r}) - \hat{f}(\boldsymbol{r})]^2 , \tag{1}$$

and a regularization term, $e_S(\boldsymbol{r})$, dependent on the spatial derivatives of the motion field. A constant term, γ_I, is used to weight the strength of the image matching component relative to the regularization component. The overall estimation problem is to find a motion field consistent with elastic material properties that best matches the deformed volume to the reference volume via a minimization of:

$$E_{tot} = \sum_{\boldsymbol{r}} [e_I(\boldsymbol{r}) + e_S(\boldsymbol{r})] . \tag{2}$$

We describe the regularization function as the strain energy of a linearly elastic uniform isotropic material. We may express the strain energy at a given voxel by the relation [2]:

$$\begin{aligned} e_S(\boldsymbol{r}) = {} & \frac{\lambda}{2}(u_x + v_y + w_z)^2 + \mu(u_x^2 + v_y^2 + w_z^2) + \\ & \frac{\mu}{2}(u_y^2 + u_z^2 + v_x^2 + v_z^2 + w_x^2 + w_y^2 + 2u_y v_x + 2u_z w_x + 2v_z w_y) \end{aligned} \tag{3}$$

where we use the notation for partial derivatives: $u_x \equiv \partial u / \partial x$, and have omitted $\boldsymbol{r}$ from the derivative terms to simplify notation. The terms, λ and μ, are elastic weighting terms called the Lamé constants. These can be written in terms of intuitive physical parameters, *E*, called the Young's elasticity modulus and ν, called the Poisson ratio:

$$E = \frac{\mu(3\lambda + 2\mu)}{(\lambda + \mu)} \text{ and } \nu = \frac{\lambda}{2(\lambda + \mu)} \quad (4)$$

E relates the tension of the object to its stretch in the same direction, and ν is the ratio between lateral contraction and axial extension. As a simple example, consider the uniaxial stretching of a rectangular object in two dimensions. A change in length along the direction of force from L to $L + dL$, and a corresponding length change along the perpendicular axis from S to $S + dS$ will be described by the Poisson ratio as follows: $dS/S = -\nu(dL/L)$.

It can be seen that the λ term in the equation penalizes non-zero divergence and the μ term penalizes sharp discontinuities in the motion field. For highly incompressible fields, the Poisson ratio approaches a maximum of 0.5, which yields a divergence term, λ, much larger than the μ term. In the limit of a completely incompressible material, the Poisson ratio is exactly 0.5 and any deformation will be volume preserving. Conversely, stretching a compressible material will increase volume and squeezing it will decrease the volume.

A formulation based on continuum mechanics like this one allows us to more intuitively set weighting factors which better model the expected deformations exhibited by an object being imaged. For example, in imaging of the heart, it is known that myocardial tissue is nearly incompressible [3]. Therefore, it should be expected that regularization weighting terms representing a Poisson ratio close to 0.5 would be most appropriate to describe the deformation of this tissue.

Minimization of the overall energy function is achieved by using a Taylor series expansion of the motion field and the calculus of variations on the resulting functional. Assuming the true motion field is $\boldsymbol{m}$, and the current estimate is $\tilde{\boldsymbol{m}}$, then a Taylor series approximation of $\hat{\boldsymbol{f}}(\boldsymbol{r})$ can be expressed in terms of a delta motion field, $\delta\boldsymbol{m} = \tilde{\boldsymbol{m}} - \boldsymbol{m}$, as $\hat{\boldsymbol{f}}(\boldsymbol{r}) = \boldsymbol{f}_1(\boldsymbol{r} + \tilde{\boldsymbol{m}}) - \nabla \boldsymbol{f}_1(\boldsymbol{r} + \tilde{\boldsymbol{m}})\delta\boldsymbol{m}$. Substituting the expression, $\tilde{\boldsymbol{m}} - \delta\boldsymbol{m}$, for $\boldsymbol{m}$ in the constraint equations results in a quadratic functional in $\delta\boldsymbol{m}$ that can be minimized via the calculus of variations [4]. The resulting Euler-Lagrange equations are solved using finite differencing techniques and a conjugate gradient method. For the simulations presented in this paper, Neumann boundary conditions were enforced, which constrains various components of the motion field gradient at the volume edges [1]. Solution to the overall problem is carried out in a two-step process involving two loops. In the outer loop, the current estimate of the motion field, $\tilde{\boldsymbol{m}}$, is used in the non-linear calculation of the current deformation volume, $\hat{\boldsymbol{f}}(\boldsymbol{r})$. Then, in an inner loop, the linear approximation is used in a conjugate gradient algorithm to compute the best $\delta\boldsymbol{m}$ satisfying the constraint equations. This delta motion field is then added to the current total motion field and the process is repeated. Further details on the overall motion estimation technique may be found in [5], [6]. Note that the linear approximation used in the Taylor series approach assumes that the maximum norm of $\delta\boldsymbol{m}$ is relatively small, else the algorithm would have difficulty converging to the true motion field, $\boldsymbol{m}$. We have found that for the simulations presented here, the assumption is valid. For cases where the image deformation is too large for the algorithm to converge to the correct motion field, a multi-scale approach may be used [6].

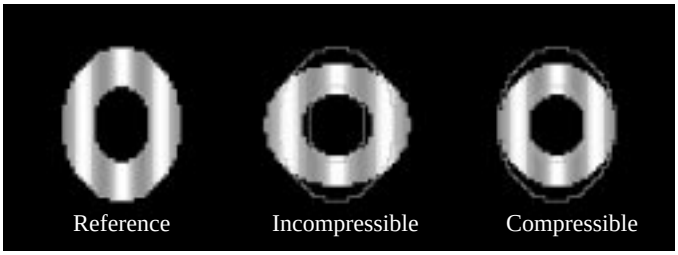

Fig 1. Hollow Ellipsoid Model. Central slice through the reference volume (left), which represents the volume in the deformed state. The source volume used in an incompressible deformation of the reference is seen in the middle; the source volume used in a compressible deformation is also shown (right). An edge map of the reference volume is overlaid on both source volumes to show the relative motion.

III. Results

To test the hypothesis that properly chosen elastic parameters can improve a motion estimation algorithm, a 3D hollow ellipsoidal phantom was created. The phantom was defined using a 64×64×16 voxel volume. Background voxels were set to zero. In order to test whether the algorithm could track features in the phantom, voxels within the boundaries of the inner and outer ellipsoids were set to an intensity governed by a sinusoidal pattern varying along the X-axis.

The model was allowed to deform into two different configurations. The first of these represents an incompressible deformation, where expansion along one axis was matched by contraction along the other. In the second configuration, the phantom contracted along one axis only, thus representing a compressible deformation. More exactly, the boundaries of the inner and outer ellipsoids for either configuration are defined by the equation:

$$\frac{x^2}{(\alpha_x a)^2} + \frac{y^2}{(\alpha_y b)^2} + \frac{z^2}{(\alpha_z c)^2} = \{A_i, A_o\} \quad (5)$$

where a, b, c describe the ellipsoid size along each axis, A_i, A_o are parameters controlling the global size of the inner and outer boundaries, and $\alpha_x, \alpha_y, \alpha_z$ represent stretch factors that can be used to describe a deformation. The sinusoidal voxel intensity relation may be similarly defined to properly account for deformation of the ellipsoid:

$$B + C\cos\left(\frac{\pi x}{3\alpha_x a}\right) \quad (6)$$

Fig. 1 shows a slice through the reference and source volumes for the incompressible and compressible cases. The source volumes define the undeformed configurations when all stretch factors are set equal to one. The reference volume represents the deformed configuration where at least one of the stretch factors is not equal to one. For the incompressible deformation, $\alpha_x = 0.8, \alpha_y = 1.25, \alpha_z = 1.0$; for the compressible deformation, $\alpha_x = 1.0, \alpha_y = 1.25, \alpha_z = 1.0$. Use of this type of deformation allows an analytical expression for the actual motion field.

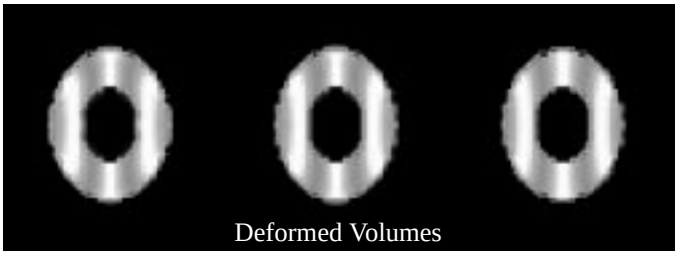

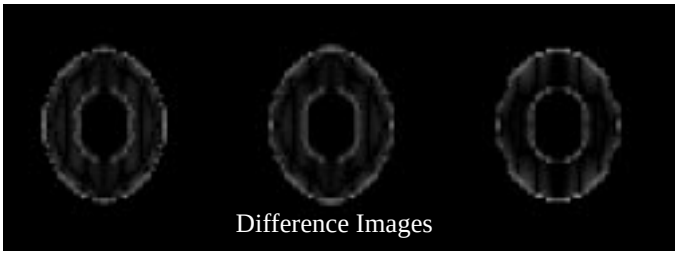

Poisson ratio=0.495	Poisson ratio=0.48	Poisson ratio=0.0
Motion Err=12478	Motion Err=8851	Motion Err=11459
Img Err= 151	Img Err= 123	Img Err= 193

Fig 2. Incompressible Deformation Results. Deformed volumes for the incompressible case using three different values of the Poisson ratio. Deformed volumes and an edge map of the reference volume shown in the top row indicate that the algorithm worked fairly well in all cases. Subtleties between the models are more evident in the difference images between the reference and the deformed volumes, shown in the bottom row. Since the material is incompressible, one would expect a modeled Poisson ratio closest to 0.5 to perform the best. Comparing the images and the figures of merit, it is seen that modeling the material as too compressible (Poisson ratio=0) produces inferior results. However, modeling the material as too incompressible also appears non-optimal.

Assuming the center of expansion and the ellipsoid center are at the origin, this is:

$$u = x(\alpha_x - 1),\ v = y(\alpha_y - 1),\ w = z(\alpha_z - 1) \qquad (7)$$

The motion estimation algorithm was run for a range of physically valid Poisson ratios (between 0 and 0.5), and the accuracy of the estimated motion field was calculated. As a figure of merit, we use the magnitude difference between estimated and true motion fields within the region of the ellipsoidal shell. The sum of squared difference between the reference and the deformed volumes is also calculated as a second figure of merit.

Fig. 2 shows the resulting deformed volumes and difference images for three different values of the Poisson ratio. In all cases, Young's modulus was set to 1.0 and the same image weighting term, $\gamma_I = 40$, was used. It is first seen that the algorithm performed fairly well for all cases shown here. For example, the voxel size for this phantom is 2×2×4 mm and the motion error was calculated over 6872 voxels representing interior the source ellipsoid. Therefore, the average motion error magnitude for the worst case in this example was still just 12478/6872 = 1.8 mm, or less than one voxel dimension. The main point of the figure though, is that it shows the expected result that modeling the material as too compressible, where $\nu \approx 0$, will result in some deformation artifacts. These are

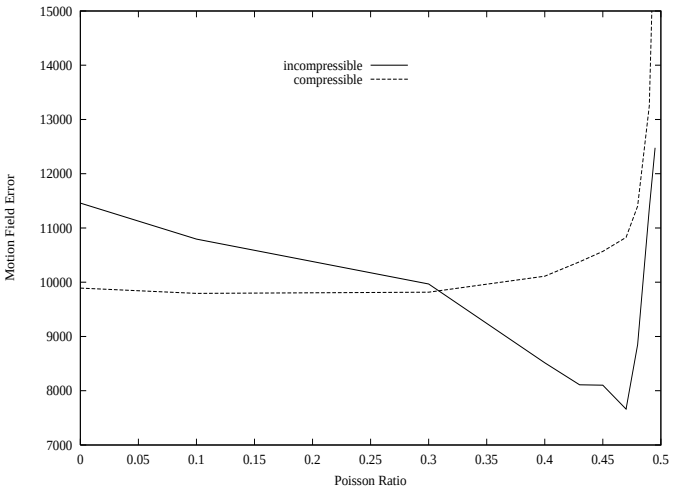

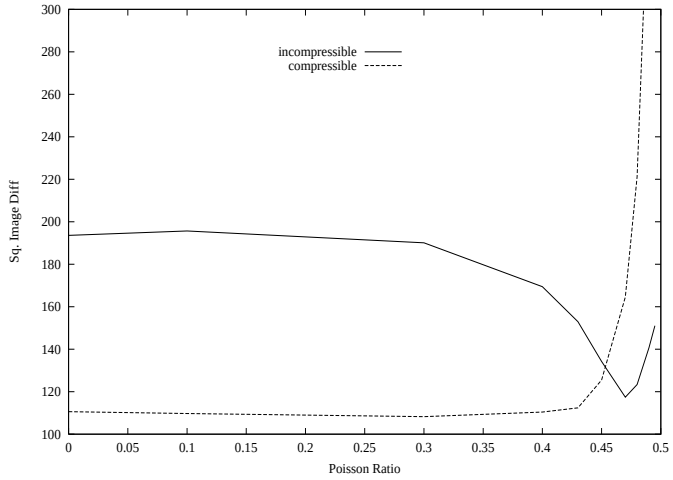

Fig 3. Motion Estimation Results. Estimation error vs. Poisson ratio for incompressible and compressible deformations. In both cases, using a Poisson ratio that matched the true value in the estimation algorithm produced better results.

especially evident by comparing the difference images in the bottom row. On the other hand, a somewhat unexpected result is seen in that modeling the material as too incompressible can also be non-optimal. Similar behavior is seen in the case of the compressible deformation.

Figure 3 plots the motion estimation error verses different values of the Poisson ratio for the incompressible and compressible simulation cases. It is seen that in general, for the incompressible case, choosing a Poisson ratio near 0.45, which represents a fairly incompressible material, appears to produce the best motion estimate and deformed volume. For the compressible case, choosing a Poisson ratio closest to 0.0 appears best. This behavior verifies the assumption that matching the elastic material parameters in the strain energy of the motion estimation algorithm to the actual elastic properties of the underlying deforming object will improve the estimated motion field.

The unexplained slight discrepancy between the algorithm's optimal performance at $\nu \approx 0.45$ rather than $\nu \approx 0.5$ for

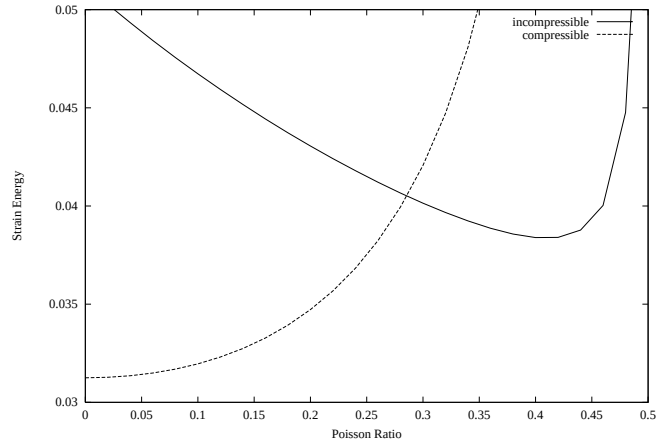

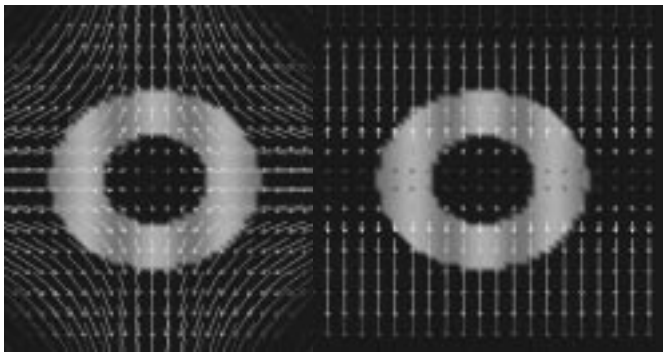

Incompressible Motion Compressible Motion

Fig 4. Analytical Strain Energy For True Motion Field. Strain energy vs. Poisson ratio for incompressible and compressible motion fields (top). Motion fields for the simulated incompressible and compressible deformations are seen in the bottom row. For the compressible case, minimum strain energy occurs for a Poisson ratio equal to zero. For the incompressible case, the minimum occurs at a value near 0.45. These results are in agreement with the motion estimation results in Fig. 3.

the incompressible case may be understood by considering the strain energy of the true motion field for different values of the Poisson ratio. For the incompressible case of pure dilation along the X and Y axis, the ratio of lengths for line segments in the source to deformed volumes is given by α and $1/\alpha$ for the X and Y axes, respectively, where α is a stretch factor. Here, a stretch factor of 0.8 was used, and the resulting strain energy has only two non-zero terms, $u_x = -0.2$, and $v_y = 0.25$. For the compressible case of a true object characterized by a Poisson ratio, $\nu = 0$, the stretch is only along the Y axis. The only non-zero term in the strain energy function in this case is $v_y = 0.25$.

Using these motion fields, we can plot the resulting strain energy as we vary the Poisson ratio. The results are seen in Fig. 4, along with the true motion fields for the compressible and incompressible deformations. Vectors in the motion field represent the direction and magnitude of the motion component in the displayed image plane. The plot shows that for the compressible deformation, the minimum strain energy occurs at a Poisson ratio equal to zero. However, for the incompressible

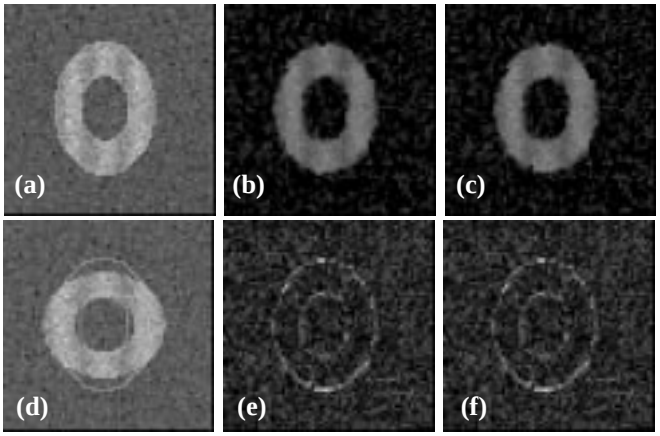

Fig 5. Motion Estimation Results-Noisy Case. Noisy reference volume (a), source volume (d), and deformed volumes using $\nu = 0$ (b) and $\nu = 0.45$ (c). Using the less compressible model produced a deformed volume with less motion field error (10192 vs. 14340) and less image matching error (848 vs. 950). Squared difference images between the noiseless reference and the deformed volumes are seen in (e), where the compressible model was used, and in (f), where the incompressible model was used.

case, it is seen that the minimum occurs not at 0.5, but at a value near 0.45. This characteristic is consistent with the motion estimation results. That is, the motion estimation algorithm appears to favor the motion field configuration with the minimal strain energy.

For matching volumes where image noise is present, the material model parameter selection becomes more crucial. Here the restraining properties of the elastic model are useful for preventing false matches between spuriously correlated voxel intensities in the source and reference volumes. An

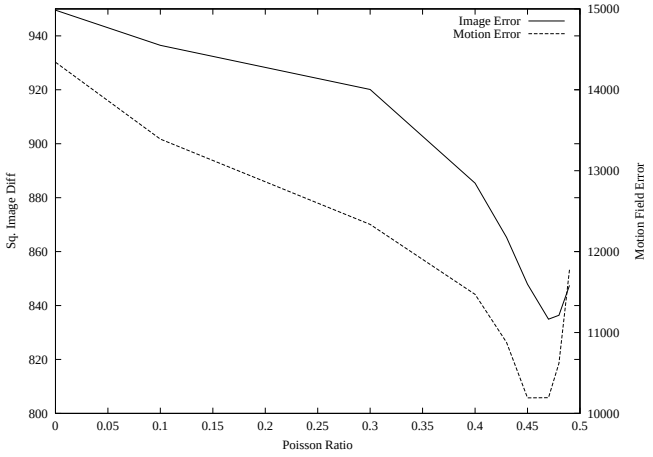

Fig 6. Motion Estimation Results-Noisy Case. Error vs. modeled Poisson ratio shows same trend as the noise-free case (Fig 3). Optimal results are obtained using a strain energy model that matches the true material characteristics.

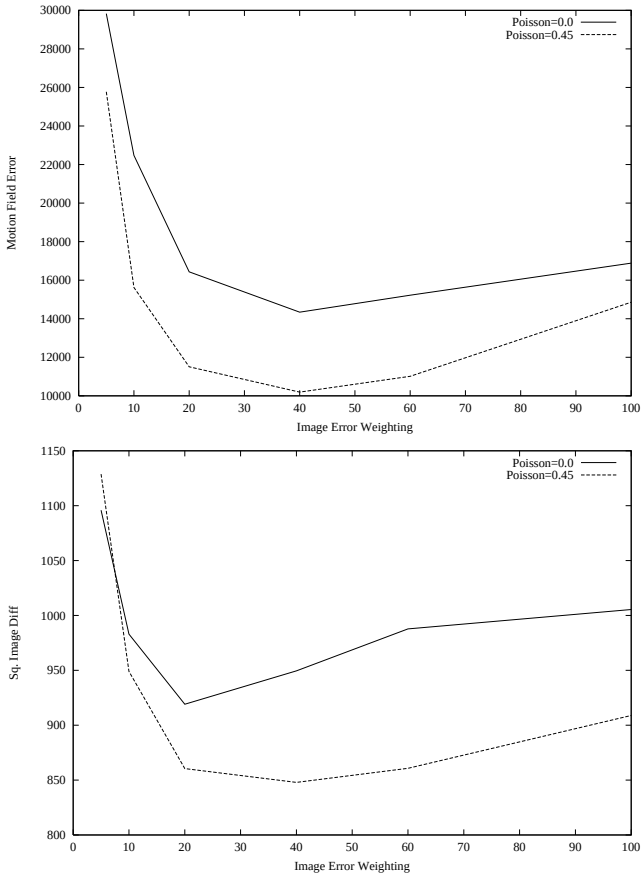

Fig 7. Image Weighting Effects-Noisy Case. Performance of the motion estimation algorithm on the incompressible noisy case using different image error weighting terms, γ_I. This term can be thought of as changing the driving force which makes the elastic volume deform. Too little force and the source volume will not deform enough to adequately match the reference. However, too large a weighting drives the algorithm to match spurious noise spikes, and thus increase the error figures of merit. Regardless of the image weighting used, the importance of choosing appropriate elastic parameters is evident.

example of this characteristic can be seen by comparing the results of using the incompressible phantom where additive Gaussian noise has been included in both the reference and source volumes. Seen in Fig. 5, the estimation using a Poisson ratio representing a fairly incompressible material ($\nu = 0.45$) produced superior results to the estimation using a compressible parameter ($\nu = 0$). Comparing the squared image difference between the deformed volume and noise-free reference, a 12% increase in error results when using the more compressible parameter. Likewise, using the flow magnitude error measure, the more compressible model produced a flow field with 41% greater error. Fig. 6 summarizes the noisy results for other values of the Poisson ratio. It is seen that the performance of the algorithm in the noisy case is similar to the noise-free result.

Fig. 7 gives information regarding the effect of changing the image error weighting term, γ_I. Recall that the difference between the reference and the deformed source volumes serves as the driving force which further deforms the source volume in an effort to better match the two. Increasing γ_I thus forces the source volume to stretch "harder" to match the reference. The figure plots the error between the deformed noisy volume and the true, noiseless reference, as well as the motion field error magnitude for various image error weights in an incompressible test case. Two different Poisson ratios are used: 0 and 0.45. It is seen that for very low values of γ_I, the error measures are large for both modeled Poisson ratios. Here, there is simply not enough force to adequately stretch the source volume into the shape of the reference. However, at the other extreme, too great a weighting on the image matching criterion encourages the algorithm to match not only the general shape between the two volumes, but also to match spuriously correlated noise spikes as well. It is desirable to use only as much image matching force as necessary, and use regularization forces from the strain energy to prevent physically unrealistic deformations. This is more likely to occur when we have appropriately modeled the true elastic behavior of the deforming material.

IV. Discussion

Results lead us to believe that by more accurately modeling the physical elastic properties of cardiac tissue and other structures within the field of view in a cardiac data set, we may obtain a more accurate estimate of the motion field describing the non-rigid deformation. The results also help to understand formulations like those of Song. They used the following regularization function composed of a divergence-free component weighted by γ_D, and general smoothness component weighed by γ_S:

$$e_S(\boldsymbol{r}) = \gamma_D(u_x + v_y + w_z)^2 + \gamma_S(u_x^2 + u_y^2 + u_z^2 + v_x^2 + v_y^2 + v_z^2 + w_x^2 + w_y^2 + w_z^2) \quad (8)$$

Comparing Song's regularization function to the strain energy function used in this paper, one can see similar components. In fact, it can be shown that the resulting Euler-Lagrange equations are identical if we set $\gamma_S = \mu/2$, and $\gamma_D = (\mu + \lambda)/2$. The advantage of using the strain energy form is that we obtain extra intuition knowing that the Lamé constants can be related to real physical phenomena seen in elastic materials. For example, the Poisson ratio for all known elastic materials is a positive number between 0 and 0.5. Using the relation of equation (4), Song's smoothness term must therefore always be weighted less than the divergence term if we wish to model physically plausible elastic material behavior. This may explain why poor results are obtained if the motion field is over-smoothed, as was demonstrated by Gorce, et. al. in their investigation of the effects of different weightings of smoothness and divergence penalties in deformable motion estimation algorithms [7]. That is, motion fields using a relatively large γ_S value implicitly imply that a negative or small value for the Poisson ratio is assumed. If the deforming material is truly incompressible, we would then expect the motion estimation algorithm to produce inferior results using a large γ_S.

We note that the strain energy model used here assumes infinitesimal displacements. In fact, this explains why the strain energy for a motion field representing an incompressible deformation does not obtain a minimum for a Poisson ratio of 0.5. We see that in our simple example using an incompressible stretch ratio of 0.8, that the motion field divergence does not sum to zero (i.e $u_x + v_y + w_z = 0.05$). Only in the case of infinitesimal displacements does the divergence approximate zero [8]. For small, but finite displacements, like the example used here, the non-zero divergence component can add appreciably to the strain energy function as the Poisson ratio, and likewise the λ term increases. It is known that the relative displacements, or strain, seen in the deforming heart can have large stretch factors similar to the values used in this paper on the ellipsoidal phantom [9]. Strain energy models which include higher order terms from the strain tensor may therefore merit further investigation. These models would more accurately match the motion estimation regularization function to the underlying elastic behavior; however, because they involve higher order terms of the motion field spatial derivatives, they would be more computationally costly and perhaps more sensitive to noise [10]. On the other hand, it is known that cardiac tissue exhibits considerable non-linear elastic behavior which is not modeled by a finite strain model that includes higher order terms, so the simple infinitesimal strain energy model with partially compressible assumptions may be just as sufficient a model to regularize a motion field.

The focus of this paper has been how to properly choose *regularization* weighting terms in the overall cost function against each other to best constrain a motion field for a specific type of deforming material. We have only touched on the other free parameter in the cost function, γ_I, which weights the regularization cost against the image matching component. Whereas use of an elastic material model is fairly straightforward for the regularization terms, finding a physical analogy to the "driving force" of the image difference term is more difficult. For the case of cardiac data, the actual force driving the cardiac tissue to deform is a combination of active muscle contraction and hydrostatic pressures. Relating these forces to a weighted voxel difference would require a more detailed model. Until such a model is available, we have little alternative but to empirically choose image weighting terms that give reasonable matches. Fortunately, as was displayed in Fig. 7, the choice of an optimal image weighting term does not appear to be a parameter that needs to be finely tuned, for similar performance is obtained using a wide range of γ_I values.

V. Summary

Results show that by more accurately modeling the physical elastic properties of a relatively simple deforming ellipsoidal phantom, we may obtain a better estimate of the vector field describing the motion. We hope that by better understanding the behavior of the estimation algorithm for simple materials, we can improve its performance for describing the motion field demonstrated by a more complex object, as would be seen in the data from a gated cardiac study. Results indicate, for example, that in order to better follow features for incompressible cardiac tissue, then this tissue should be characterized by a material model that enforces incompressibility. We acknowledge that the elastic properties of cardiac tissue are certainly different from the adjacent blood pool and lung tissue. However, by separately describing each tissue class with appropriate physical elastic parameters, it is hoped that feature tracking may be improved for gated cardiac PET.

VI. Acknowledgments

This work was supported in part by the National Heart, Lung and Blood Institute of the U.S. Department of Health and Human Services under grant P01-HL25840; and in part by the Director, Office of Energy Research, Office of Biological and Environmental Research, Medical Applications and Biophysical Research Division of the U.S. Department of Energy under Contract DE-AC03-76SF00098.

VII. References

[1] S. M. Song and R. M. Leahy. Computation of 3-D velocity fields from 3-D cine CT images of a human heart. *IEEE Trans Med Imag*, 10(1):295–306, 1991.

[2] A. Love. *A Treatise on the Mathematical Theory of Elasticity*. Dover Publications, New York, 1927.

[3] K. D. Costa, P. J. Hunter, J. S. Wayne, L. K. Waldman, J. M. Guccione, and A. D. McCulloch. A three-dimensional finite element method for large elastic deformations of ventricular myocardium: II - prolate spheroidal coordinates. *Trans. ASME*, 118:464–472, 1996.

[4] B. K. P. Horn. *Robot Vision*. The MIT Press, Cambridge, Massachusetts, 1986.

[5] G. J. Klein. Forward deformation of PET volumes using non-uniform elastic material constraints. In A. Kuba and J. Attila, editors, *Information Processing in Medical Imaging, 16th Annual Conference*, volume 1613, pages 358–363. Springer, 1999.

[6] G. J. Klein. Deformable models for volume feature tracking. Report LBNL-43257, Lawrence Berkeley National Laboratory, 1999. (Ph.D. Thesis).

[7] J. Gorce, D. Friboulet, and I. E. Magnin. Estimation of three-dimensional cardiac velocity fields: Assessment of a differential method and application to three-dimensional CT data. *Med. Image Anal.*, 1(3):245–261, 1997.

[8] R. S. Rivlin. Large elastic deformations of isotropic materials. I. *Proc R Soc Lond A*, 240:459–490, 1948.

[9] K. R. Walley, M. Grover, G. L. Raff, J. W. Benge, B. Hannaford, and S. A. Glantz. Left ventricular dynamic geometry in the intact and open chest dog. *Circ. Res.*, 50(4):573–589, 1982.

[10] F. D. Murnaghan. *Finite Deformation of an Elastic Solid*. Chapman & Hall, Limited, New York, 1951.